Journal of Materials Chemistry

Cite this: J. Mater. Chem., 2011, 21, 13594

www.rsc.org/materials

PAPER

Impact of initial solvent on thermal stability and mechanical properties of recombinant spider silk films†

Kristina Spiess,[a] Roxana Ene,[b] Caroline D. Keenan,[c] Jürgen Senker,[c] Friedrich Kremer[b] and Thomas Scheibel*[a]

Received 19th April 2011, Accepted 29th June 2011
DOI: 10.1039/c1jm11700a

Spider silk fibers are one of the most remarkable biopolymers displaying a unique combination of mechanical properties, biocompatibility and biodegradability. The recombinant production of spider silk proteins now allows the processing of silk proteins into novel materials with the aim of future applications. Here, we analyzed films made of a recombinantly produced, engineered spider silk protein with a sequence derived from the dragline silk protein ADF4 of the European garden spider *Araneus diadematus*. An influence of different initial solvents (aqueous buffer, hexafluoro-2-propanol and formic acid) on certain film properties was identified in as cast as well as methanol post-treated films: while no significant effects on the films' thermal stability were observed, a significant influence on their mechanical properties could be shown. Interestingly, solvent-induced effects were sustained after methanol post-treatment and could be correlated with the presence and arrangement of secondary structure elements. Insights into molecular orientation of individual structural elements within the films upon applied load were revealed by combined polarized IR spectroscopy and mechanical measurements.

Introduction

Silk-based materials could improve many devices in the field of biomedical to optical, sensoring and other technical applications.[1–5] Silks are a class of fibrous proteins, produced by arthropods, with silk fibroin from the silkworm *B. mori* and diverse spider major ampullate (dragline) silks being the best analyzed ones.[6–9] The reason for silk's versatile applicability is based on its biocompatibility, biodegradability, mild processing conditions in combination with excellent mechanical properties.[1,4,10]

Especially spider dragline silk, which comprises the frame and radii of an orb web, is acknowledged for its high toughness, unique amongst natural and artificial fibers.[11,12] Many studies elucidated the molecular blueprint of silk proteins employing methods such as X-ray diffraction,[13–15] NMR[16,17] as well as infrared and Raman spectroscopy,[18,19] among others. In comparison to silkworm silk consisting of three proteins with quite different molar masses (heavy and light chain fibroins and P25),[4] dragline silk mainly consists of two similar-sized proteins,[20,21] both exhibiting a characteristic amino acid sequence with a block copolymer-like arrangement of distinct amino acid motifs.[11,22,23] Among these motifs are blocks of 6–8 alanine or alternating glycine–alanine residues which preferentially fold into β-sheet structures in the fiber. Characteristically, the sheets stack to form regular crystallites, providing high tensile strength and stiffness.[24,25] Glycine-rich motifs (*e.g.* GPGQQ GPGGY) have been assigned to more flexible structural elements like β-turns, 3_1-helices and random structures.[18,26] The crystallites are interspersed in a so-called amorphous matrix with the additional presence of a fraction of oriented and pre-stressed chains.[16,27–29] Based on these findings, a three phase model has been proposed in which the highly oriented β-sheet crystallites are connected (in serial arrangement) by the pre-strained and the amorphous chains.[30] This complex hierarchical composition is thought to be the basis for the dragline silk's outstanding properties.[10] Differences in the molecular composition and arrangement might be involved in contributing to different properties (like mechanical stability) in spider dragline and silkworm silks.

Progress in developing advanced biotechnological approaches in recent years allowed the efficient recombinant production of spider silk proteins.[31–33] Mostly, a module system is applied to mimic individual motifs/domains found within the natural proteins. For example, the engineered protein eADF4(C16) consists of 16 modules derived from the consensus sequence of

[a]*Lehrstuhl Biomaterialien, Universität Bayreuth, D-95440 Bayreuth, Germany. E-mail: thomas.scheibel@bm.uni-bayreuth.de; Fax: +49 921 55 7346*
[b]*Institut für Experimentelle Physik I, Universität Leipzig, D-04103 Leipzig, Germany*
[c]*Lehrstuhl Anorganische Chemie I, Universität Bayreuth, D-95440 Bayreuth, Germany*

† Electronic supplementary information (ESI) available: Removal of HFIP upon heating of spider silk films as detected by FTIR spectroscopy (Fig. S1). Force curves of silk films from different solvents obtained by simultaneous stepwise stretching/FTIR measurement (Fig. S2). See DOI: 10.1039/c1jm11700a

the repetitive part of the dragline silk protein ADF4 of the garden spider *Araneus diadematus*.[34] Apart from studying the complex process of fiber formation,[35–37] recombinant proteins offer the possibility to analyze assembly into non-fibrous morphologies like spheres, foams or films.[3,9]

Silk films have shown high potential as promising new biomaterials, particularly in supporting cell growth and proliferation,[1,2,32] tissue engineering,[8] controlled (drug) release[38–40] or as biocompatible photonic devices.[41,42] Diverse approaches to modify and functionalize films of silkworm or recombinant spider silk were reported to further adjust their properties for individual requirements.[2,43] However, most of the previous work has been done on films of regenerated *B. mori* silk fibroin (SF). SF films can be cast from solution in water[2,9] or organic solvents (such as hexafluoro-2-propanol (HFIP),[44] formic acid[45–47] or trifluoroacetic acid[46]). Analysis of these films indicated the presence of structural elements similar to those found in natural silkworm silk fibers. Depending on the processing conditions, IR- and XRD-signals typical for silk I (amorphous structures and type II β-turns) and silk II (antiparallel β-sheets) conformations were reported.[48] Several triggers like organic solvents (mostly methanol),[48–51] temperature[51,52] or shear stress[50,53,54] can induce the formation of β-sheet structures in silkworm silk films. Further, the degree of crystallinity can be influenced by varying the concentration of methanol and the incubation time with methanol,[1] casting temperature[51,55] or water annealing.[48]

Although silk fibroin and spider silk proteins share some physico-chemical characteristics, like a highly repetitive primary sequence and a hierarchical structural composition involving crystalline and non-crystalline regions, they also reveal distinct differences. The amino acid motif forming β-sheet crystallites is $(GAGAGS)_n$ in *B. mori* silk,[4,23] but A_n in the spider dragline silk protein ADF4 as well as in the engineered recombinant protein eADF4(C16).[10,14,34] Moreover, eADF4(C16) displays a lower molecular weight (M_w 47 kDa), a lower hydropathicity and less charges than heavy chain SF.[34] These differences have recently been shown to result in an altered assembly behaviour of both proteins upon salting-out and in different mechanisms of drug release from microspheres made of SF or eADF4(C16).[56,57] Regenerated SF solutions represent a heterodisperse system, consisting of a mixture of heavy and a light chains (M_w 392 kDa and 26 kDa) and P25 (M_w 25 kDa),[4,23] while biotechnologically produced eADF4(C16) is monodisperse with reproducible quality, which has a significant impact on processing.[10,31]

Previously, eADF4(C16) has been cast into transparent films from HFIP solutions. These films were analyzed according to their structure,[49,58,59] effect of post-treatment with alcohols[58] and kosmotropic ions,[49] and their microhardness.[60] After methanol treatment, β-sheet stacks assembled into regular nano-crystals with dimensions between 2 and 40 nm and an average size of 7–8 nm.[59] Other reports on films of recombinantly produced spider silk proteins focused on structural features[49,61,62] and their applicability as cell supporting devices[62–64] or for silicification.[65]

Here, we investigated systematically the influence of different initial solvents (HFIP, formic acid and aqueous buffer) on secondary structure and thermal and mechanical stabilities of eADF4(C16) films, without further treatment (as cast) and after methanol post-treatment. Some of the observed effects correspond well to mechanisms already known for *B. mori* SF films, but others are unique for our system. A combined FTIR/mechanical analysis allowed an elucidation of the molecular arrangement and force dissipation in films cast from the different initial solvents, stressing the importance of interstitial solvent molecules and the arrangement of β-sheet structures in addition to their overall amount in the respective films.

Results and discussion

Casting of silk films from different solvents: implications on the secondary structure

Silk films can be cast from different aqueous or organic solvents (mostly HFIP, formic acid (FA) or trifluoroacetic acid[44–47]). It has been shown that certain solvents might affect the proteins' secondary structure. Here, we employed buffered aqueous solution (*aq*), HFIP and FA as solvent. The secondary structure of eADF4(C16) in solution was determined previously,[58] revealing a mainly unstructured conformation in buffered aqueous solution. No differences were observed by employing different buffers at identical pH values (5 mM sodium phosphate pH 8, 10 mM Tris–HCl, pH 8 and 5 mM ammonium bicarbonate pH 8). In contrast, HFIP induces α-helical structures.[58] The secondary structure of eADF4(C16) dissolved in FA could not be determined due to the high intrinsic optical activity of FA.

In order to analyze the effect of the starting solvent on the secondary structure after film formation, films were cast from the respective solvents and characterized by FTIR spectroscopy and high-resolution solid-state NMR spectroscopy. In order to prevent the formation of salt crystals upon drying of the aqueous solution, ammonium bicarbonate was chosen as buffer system due to the known volatility of its components. In the obtained FTIR spectra, the amide I (1600–1700 cm^{-1}) and amide II (1500–1580 cm^{-1}) bands were analyzed, representing mainly C=O stretching vibrations of the amide backbone (amide I) and N–H bending in combination with C–N asymmetric stretch vibrations (amide II).[51,69,70] As expected, the absorption bands in these regions of as cast films differed depending on the solvent used. HFIP films showed spectra dominated by maxima at 1654 cm^{-1} and 1548 cm^{-1} (Fig. 1a), which can be assigned to α-helical/random coil conformations as reported previously.[43,49] In contrast, films cast from FA solution revealed an additional maximum at 1627 cm^{-1} based on the presence of β-sheet structures. Strikingly, spectra recorded for buffered films differed depending on the local region of the film being analyzed. Upon cutting the films into strips for analysis, certain strips (we named these type I) revealed spectra similar to those from as cast films from HFIP. In comparison, spectra of other strips (type II) of buffered films revealed a broadening of the amide I band towards lower wavenumbers, indicating higher contributions from β-sheet structures (as seen at 1616–1636 cm^{-1}).[51] The two different regions are likely due to an inhomogeneous evaporation of the buffer. Importantly, no crystals of the salt (ammonium bicarbonate) could be detected in the films.

The secondary structure composition was further analyzed by Fourier self-deconvolution (FSD).[51] Selected FSD spectra are shown in Fig. 1 for as cast HFIP (c) and type II buffered films (d). The calculated amounts of β-sheets in as cast films are 21% (HFIP), 25% (type I *aq*), 30% (type II *aq*), and ~32% (FA), with

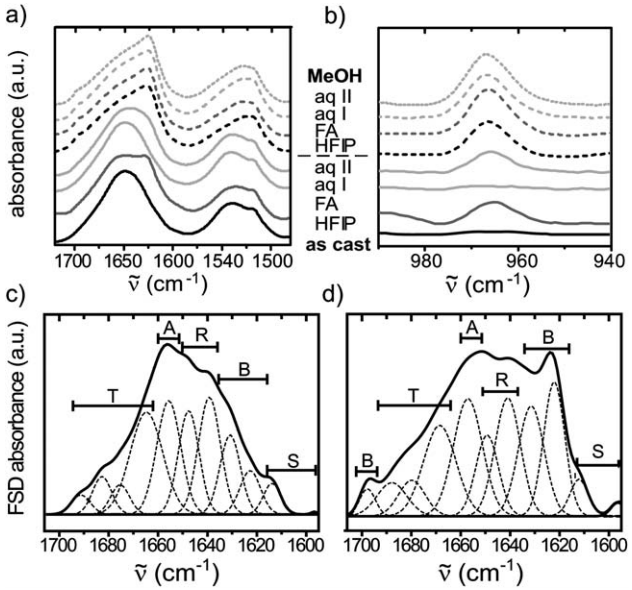

Fig. 1 Influence of different solvents on secondary structure of eADF4 (C16) films. FTIR spectra of films were taken before ("as cast", solid lines) and after methanol treatment (MeOH, dotted lines) as indicated. (a) FTIR spectra focused on the amide I and II regions; (b) Focus on the fingerprint region 1000–930 cm^{-1}, with the peak at ~965 cm^{-1} reflecting polyalanines in β-sheet structure. (c and d) Fourier self-deconvolution (FSD) of FTIR spectra of as cast HFIP (c) and buffered type II (d) films. T: turns, A: α-helix, R: random coil, B: β-sheets, S: side chains/others; aq I and II: different regions (types I and II) in films from buffered solution.

HFIP films displaying the highest amount of α-helices (Table 1). This result is in good agreement with previously described effects of the individual solvents on the secondary structure of proteins. In fluorinated alcoholic solvents (like HFIP) proteins tend to adopt α-helical structure,[58,71,72] while a β-sheet inducing effect of FA has been reported for some proteins,[45–47] indicating general features of these solvents. Both solvents have been described to act *via* interaction of the solvent molecules with the polypeptide backbone/side chains and/or by influencing the hydration shell of the proteins.[46,47,71] For formic acid, a stabilization of the protein in a compact conformation has been reported, thereby facilitating the formation of thermodynamically stable β-sheets after solvent evaporation.[46] Furthermore, we observed a clear dependency of the secondary structure on water content/humidity in as cast films from FA and buffered aqueous solution (data not shown); therefore, in all experiments the relative humidity was kept constant at 30% relative humidity.

Post-treatment with methanol is known to induce β-sheet formation in silk films from regenerated *B. mori* SF[1,48,51] as well as eADF4(C16) films cast from HFIP.[58,59] Here, we observed an according increase in β-sheet content in films cast from either solvent, as seen in the dominant maximum at 1624 cm^{-1} in FTIR spectra (Fig. 1a), becoming the most prominent structural component after methanol treatment. Interestingly, the portion of β-sheet structure reached the same value (42.0–42.5%) in all but one sample, regardless of the structural content in the respective film before methanol treatment (Table 1). Only *aq* type I films (again, *aq* films gave rise to two different FTIR spectra depending on the film type) revealed a somewhat lower β-sheet content (Table 1). The general increase in β-sheet structures upon methanol treatment occurred at the expense of α-helical/random coil conformation, which was especially pronounced in films cast from HFIP (Table 1).

A special structural characteristic of spider silk proteins (in comparison to that of silkworm silk) is the presence of poly-alanine β-structures (β-polyalanines) which can be detected in the IR spectral region between 900 and 1000 cm^{-1} (Fig. 1b).[73] Analyzing the IR-signals in that regime revealed the presence of a peak at 964 cm^{-1} in all films except in as cast HFIP and type I *aq* films, where this peak was either absent or not significant.

In order to confirm the absence of the β-polyalanine structures in such films, solid state NMR (ssNMR) was performed. The

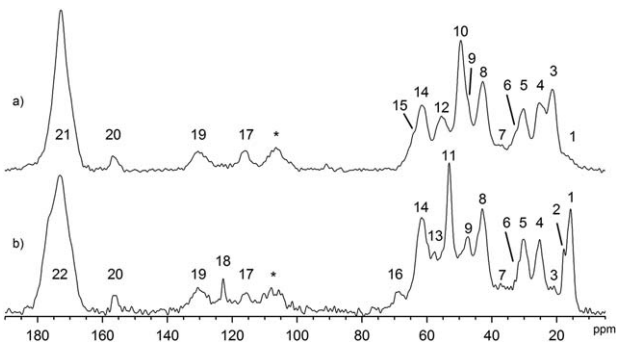

Fig. 2 $^{1}H^{13}C$ CP MAS spectra of eADF4(C16) films cast from HFIP with (a) and without (b) subsequent methanol treatment. Spectra were acquired with $\{^{19}F,^{1}H\}$[74,75] double decoupling. Spinning sidebands are denoted by asterisks and the assignment of the indicated resonances is provided in Table 2.

Table 1 Secondary structure content of spider silk films after (MeOH) or before (as cast) methanol treatment as determined by Fourier self-deconvolution of respective FTIR spectra. All calculated numbers are given in % with an error of ±2%

	HFIP		Formic acid		Aqueous buffer			
Secondary structure	As cast	MeOH	As cast	MeOH	As cast I	As cast II	MeOH I	MeOH II
β-Sheet (1616–1637 cm^{-1}, 1697–1703 cm^{-1})	21.1	42.3	31.7	42.5	25.3	30.2	37.0	42.0
α-Helix (1653–1662 cm^{-1})	18.7	7.7	11.5	9.4	14.0	13.7	12.1	8.4
Random coil (1637–1652 cm^{-1})	27.7	21.7	24.7	21.1	27.5	26.8	21.4	23.6
β-turns (1663–1696 cm^{-1})	27.8	21.9	26.9	22.0	28.0	24.4	23.3	22.0
Others (1595–1615 cm^{-1})	4.2	4.7	4.2	4.6	4.7	4.3	4.7	4.8

Table 2 Chemical shift assignments of the ^{13}C MAS spectra of eADF4(C16) films cast from HFIP with and without subsequent methanol treatment. Assignment numbers correspond to resonances as indicated in Fig. 2. RC: random coil conformation

		Gly			Ala			Pro		Ser		Tyr	Gln	HFIP
Residue		α-Helix	β-Sheet	3_1-Helix	α-Helix	β-Sheet	3_1-Helix	RC	3_1-Helix	α-Helix	β-Sheet	RC	RC	Solvent
C_α	No.	9	8	8	11	10	10	14	14	14	12	13	12	18
	δ/ppm	47.4	42.8	42.8	53.3	49.5	49.0	61.7	59.6	59.7	56.8	57.6	55.4	122.9
C_β	No.				1	3	2	5	5	14	15	7	5	16
	δ/ppm				15.7	21.2	17.8	30.2	30.2	63.3	64.2	37.4	30.2	68.8
$C_{\gamma,\delta}$	No.							4	4			19	6	
	δ/ppm							25.3	25.3			130.7	32.9	
C_{Other}	No.							4	4			$17^{C\varepsilon}/20^{C\xi}$		
	δ/ppm							47.4	47.4			116.0/156.2		
C=O	No.	22	21	—	22	21	—	21/22	22		21	—	—	
	δ/ppm	173.2	169.4	172.1	176.5	171.3	172.1	174.1	174.5		170.0	172.0	178.2	

results (Fig. 2 and Table 2) confirm and refine the FTIR data. In the HFIP as cast film (Fig. 2b), alanine residues are present in an α-helical structure with distinct peaks at 15.7 ppm (No. 1) (indicative of the alanine C_β carbon in an α-helical conformation) and 53.3 ppm (No. 11) (assigned to alanine C_α in an α-helical structure). The small resonance at 17.8 ppm (No. 2) is tentatively assigned to the C_β carbon of alanine, in a 3_1-helical conformation,[74,75] like it has been described to exist in major ampullate spider silk.[26] Peaks relating to alanine residues in β-sheet conformation are near the detection limit, correlating well with the absence of a peak at 964 cm^{-1} in FTIR spectra. After methanol treatment (Fig. 2a) the resonances are shifted down field, indicating that the alanine C_β carbon is now in β-sheet (21.2 ppm (No. 3)) structures, additionally supported by a peak at 49.5 ppm (No. 10) (assigned to alanine C_α in β-sheet conformation). The comparison of the spectra depicted in Fig. 2 demonstrates that nearly all α-helical alanine peaks have shifted to peaks representative of β-sheet arrangements. A qualitative estimate of the relative percentage of alanine residues in β-sheet conformation was determined by comparing the spectroscopic intensities of resonances 3 and 1 of Fig. 2b. Similar treatment was applied to the same resonances within methanol treated films (Fig. 2a). Results suggest that roughly one-fifth of the alanine residues adopts a β-sheet conformation within the HFIP as cast film, while estimated one-tenth of the alanine residues exists in α-helical structures within the β-sheet rich methanol treated film. Unfortunately, the broad overlap of resonances prevents similar analysis of the glycine residues.

Thermal stability

Important for any application is the stability of the respective silk film. Previously, the chemical stability of eADF4(C16) films has been investigated revealing similar properties in comparison to natural spider silk fibers which can only be dissolved in strong denaturants such as guanidinium thiocyanate.[49] Here, we analyzed the thermal stability of the films by thermogravimetric analysis (TGA) and differential scanning calorimetry (DSC). TGA (Fig. 3a and Table 3) revealed a mass loss of 4.9–7.1% in the temperature range between 32 °C and 100 °C (with T_m of 53–69 °C, Table 3), reflecting evaporation of water and/or solvent. All films showed a massive mass loss (59–68%) around 335 °C indicating thermal decomposition. An additional mass loss was detected in as cast HFIP films between 140 and 226 °C (T_m = 183 °C) and in as cast FA films between 169 and 282 °C (T_m = 197 °C). A minimal mass loss in this temperature range was also detected in methanol treated FA films (Fig. 3a, inset). However, this process cannot be properly separated from the subsequent mass loss of thermal decomposition.

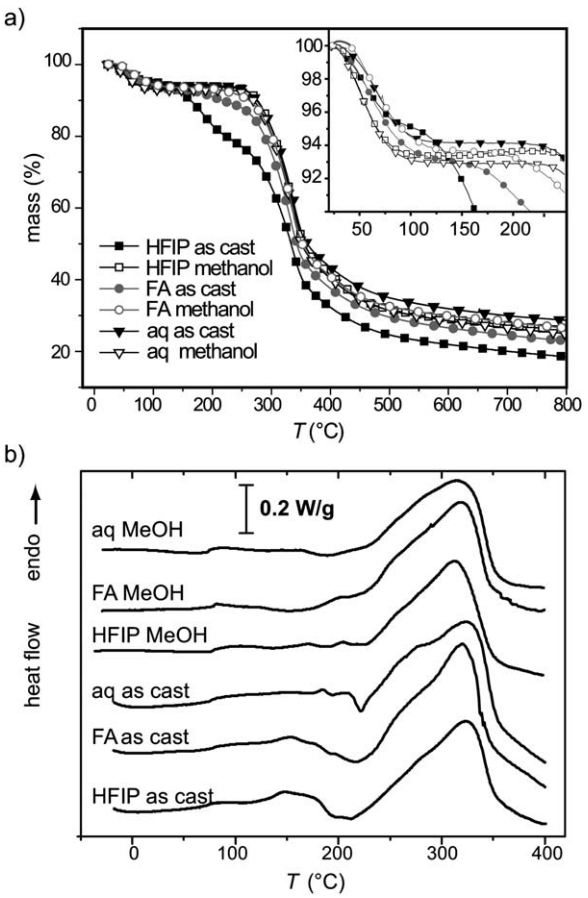

Fig. 3 Analysis of thermal stability of eADF4(C16) films with (MeOH) and without (as cast) subsequent methanol treatment. (a) TGA scans of films heated under nitrogen atmosphere at 10 °C min^{-1} from RT to 800 °C. (b) DSC scans of films heated under nitrogen flow at 5 °C min^{-1}. Samples were heated up to 110 °C, then cooled to −40 °C, followed by heating to 400 °C. For clarity, only the second heating cycle is shown. Therefore, the endothermic peak of the initial solvent loss is not visible. The shown scale bar represents 0.2 W g^{-1}.

Table 3 Overview over mass loss Δm of eADF4(C16) films as determined by TGA. The given temperature T_m reflects the temperature at which 50% mass loss of the respective transition is achieved

		1		2		3		
Solvent	Post-treatment	T_m/°C	Δm (%)	T_m/°C	Δm (%)	T_m/°C	Δm (%)	Remaining mass (%) at 800 °C
HFIP	As cast	57	4.9	183	16.8	332	59.8	18.5
	MeOH	53	6.7			335	67.5	25.8
FA	As cast	64	7.0	197	5.0	334	65.0	23.0
	MeOH	69	6.6			334	66.9	26.5
Aqueous	As cast	68	5.9			336	65.3	28.8
	MeOH	56	7.1			334	68.0	24.9

DSC scans of all films displayed endothermic peaks around 320 °C with a shoulder at ~265 to 280 °C (Fig. 3b), representing a bimodal melting/thermal decomposition of the silk films.[47,76] As cast HFIP and FA films revealed additionally broad endothermic peaks between 130 and 185 °C (HFIP) and 135–195 °C (FA). These signals were absent or significantly diminished after methanol treatment, which largely leads to elimination of the initial solvent. Together with the observed mass loss of 5% (FA) and ~17% (HFIP) in this temperature region as seen by TGA (Table 3), the observation is likely based on the evaporation of bound solvent. This hypothesis could be further confirmed by FTIR spectroscopy, where HFIP-derived signals were largely diminished above 180–200 °C (Fig. S1†). However, still interstitial solvent (mainly water) molecules are likely present in these films.

Distinct exothermic peaks were observed in all as cast films at slightly different temperatures, at 210 °C in the case of HFIP films, at 215 °C for FA films and at 221 °C for buffered films. Similar peaks have been reported for regenerated *B. mori* silk films and have been attributed therein to structural transitions from random coils/α-helices to β-sheets (*i.e.* temperature-induced β-sheet formation).[51,55] FTIR spectra of as cast eADF4(C16) films taken during heating the films confirmed this observation (Fig. 4). No according exothermic signals were found in methanol treated films, which is plausible since they have already a converted structure with higher β-sheet content in comparison to as cast films.

An additional step in DSC scans of methanol treated films was observed at 195 °C (*aq*) and 210 °C (HFIP), likely representing a glass transition similar to that previously reported for *B. mori* films.[47,51,55] The highest temperature of this glass transition was observed for HFIP films, pointing towards a slightly enhanced stability of chain interconnections in these films. Although no such step was visible in spectra of as cast films, it might be also present, but probably overlaps with peaks of solvent loss and β-sheet transition. This hypothesis is based on the fact that the temperature of such glass transition has been previously described to vary depending on the moisture content[55,77] which influences the mobility of the polypeptide chains. Concomitant with the observed mass loss in TGA, an endothermic peak below 100 °C was detected by DSC in all films, which can be attributed to initial solvent loss[78] (the data are not shown as explained in the legend of Fig. 3).

In summary, thermal analysis did not reveal significant differences between films made from different solvents. In either of the as cast films a temperature dependent β-sheet transition was observed, varying only slightly in temperature. Furthermore, decomposition occurred at the same temperature in all films, likely based on the fact that films from all solvents are rich in β-sheet structure (either induced by methanol treatment or by temperature during the DSC scan (Fig. 4)). Although the DSC scans of films of eADF4(C16) display characteristics comparable to that of films of regenerated *B. mori* SF, indicating similar molecular processes upon heating, temperatures of glass transition and thermal decomposition are significantly higher in the spider silk films compared to SF films (T_g between 195 and 210 °C for recombinant spider silk *vs.* 178 °C reported for *B. mori* silk films; decomposition of recombinant spider silk at 330 °C *vs.* 274–296 °C for *B. mori* SF).[51,55] A reason therefore might be found within the β-sheet structures of the respective films. While the β-sheet-forming primary sequence in *B. mori* SF is $(GAGAGS)_n$,[4,23] $(A)_n$ comprises the β-sheet-forming sequence in eADF4(C16).[10,34] The additional stabilization *via* hydrophobic interactions of the alanine residues might contribute to the observed higher stability in spider silk films. Different dimensions and interconnection of the β-sheet structures, which have been previously proposed to be responsible for the respective mechanical behavior,[88] could also influence the thermal stability. The observed higher stability of recombinant spider silk films could be of relevance for distinct (technical) applications.

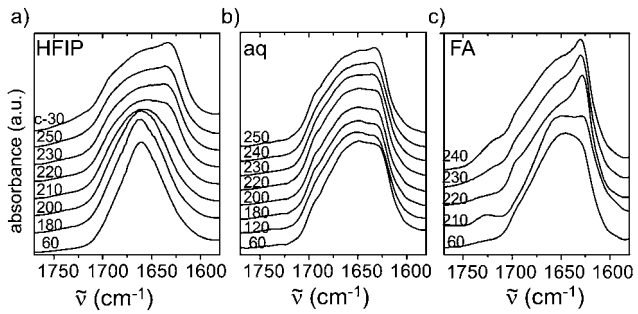

Fig. 4 Structural changes upon heating monitored by FTIR. Films cast from HFIP (a), buffered aqueous solution (b) and FA (c) were heated in a sealed cell which was placed directly under the IR beam. After subsequent cooling of the samples, films were analyzed again ("c-30 °C"), indicating the thermodynamic stability of β-sheet structures.

Mechanical properties of silk films

Next, we analyzed the influence of the initial solvent on the mechanical behavior of the silk films. All measurements were done in dry state at a relative humidity of 41 ± 1%. The two detected structurally differing regions in buffered films (*aq*) (Fig. 1) have also distinct mechanical characteristics (Fig. 5).

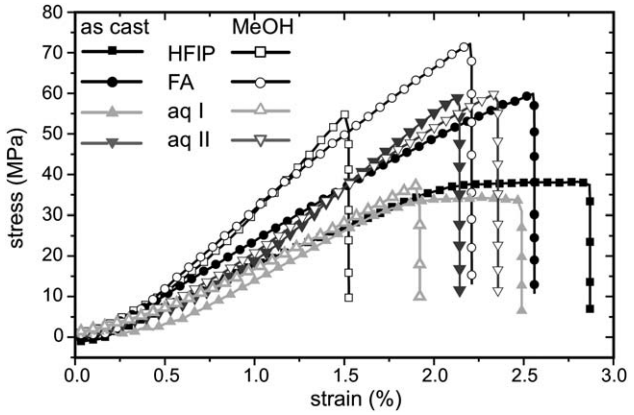

Fig. 5 Mechanical properties of eADF4(C16) films. Films cast from different solvents were tested either without (as cast, filled symbols) or after methanol post-treatment (MeOH; open symbols). Stress–strain curves were obtained using an Instron universal tester 5565 with a crosshead speed of 0.2 mm min^{-1}. The two distinct structural regions (types I and II) of aq films displayed also different mechanical properties.

While as cast *aq* type II films revealed a single linear slope followed by a sharp failure of the sample similar to as cast FA films and similar to all methanol treated films, as cast *aq* type I films revealed plastic deformation of the material upon a strain higher than 1.7–2% similar to HFIP as cast films (Fig. 5). Accordingly, the latter two films had lower *E*-moduli and tensile strength than the others (Table 4). Concomitantly, the HFIP as cast films showed ~15% higher values of elongation at break. In all cases, methanol treatment resulted in enhanced *E*-moduli and tensile strength and a decrease in elongation at break (Table 4). The strongest films in terms of toughness and tensile strength were those cast from FA (either as cast or methanol treated). While the absolute values for stiffness and elongation to break varied with relative humidity (when applying humidity other than ~40%), the general trends as well as ultimate strength were retained (data not shown).

The correlation of the presence and amount of β-sheet structure with strength and stiffness and decreasing elasticity of silk films (made of *B. mori* SF) has been shown previously,[47,79] being in agreement with the observed effect of methanol treatment on the mechanical properties of all recombinant spider silk films in this work. The β-sheets are thought to act as physical crosslinks between the molecules, thereby acting as reinforcing fillers conferring stability to the material. As a result, an increase in β-sheet structure would lead to an increase in mechanical stability (in terms of strength and stiffness) of the films. However, the secondary structural composition (as determined by FTIR) of methanol treated eADF4(C16) films was almost identical independent of the solvent used (Fig. 1), yet the films revealed clear differences in their mechanical properties. This discrepancy suggests that the individual solvents caused differences in the molecular arrangement within the films, leading to different mechanical properties while revealing the same overall portion of secondary structure elements. Further, it is possible that interstitial solvent molecules (FA, HFIP, water or MeOH) directly contribute to the properties, *e.g.* acting as plasticizers with slightly different impact.

Molecular orientation upon stretching

Based on the previous finding, we next investigated the molecular arrangement of individual secondary structure elements upon stretching by simultaneous mechanical and polarized IR measurements. The films were glued to metal holder rods of an apparatus equipped with micrometre screws for controlled stretching of the films and with a force sensor to measure the applied force (Fig. 6a). Films were stretched stepwise, and after relaxation of the material (as seen by the force curve), polarized IR rapid scan measurements were performed under equilibrium in order to study the dichroism of the material (Fig. 6b and Experimental). Due to the different experimental setup (including stepwise stretching and relaxation) the resulting stress/strain values of the films are not identical to the ones obtained by continuous tensile testing as presented above.

In the natural silk thread, a high level of orientation of the protein structures, especially of the β-sheet rich regions, has been observed, and the degree of orientation has been correlated to the fiber's mechanical properties.[15,28,80–82] Therefore, the IR transmission was measured at various polarization angles allowing the calculation of molecular order parameters (S^{mol}), in order to quantify the degree of orientation of specific transition dipole moments with respect to the sample or force axis (for details see Experimental).

Before stretching, none of the IR spectra of the films revealed dichroism, indicating that there is no preferred orientation of the molecules/structures within the films (a representative example is shown in Fig. 6c). For detailed analysis of the effect of stretching on the molecular level/arrangement, we focused on the above mentioned β-polyalanine band, especially in the region between

Table 4 Mechanical properties of eADF4(C16) films cast from different solvents with (MeOH) and without (as cast) methanol post-treatment. For each film type, at least 10 individual samples were measured to calculate a mean value

Sample		*E*-modulus/GPa	Strength/MPa	Elongation at break (%)	Toughness/kJ m^{-3}
FA	As cast	2.9 ± 0.4	60 ± 5	2.5 ± 0.4	770 ± 190
	MeOH	3.5 ± 0.3	71 ± 2	2.2 ± 0.1	790 ± 80
HFIP	As cast	2.4 ± 0.3	42 ± 4	2.9 ± 0.1	770 ± 130
	MeOH	3.3 ± 0.5	52 ± 3	1.8 ± 0.3	370 ± 150
Aqueous	As cast type I	2.2 ± 0.2	31 ± 5	2.4 ± 0.4	380 ± 110
	As cast type II	3.1 ± 0.3	51 ± 8	2.6 ± 0.8	680 ± 250
	MeOH I	2.8 ± 0.4	40 ± 5	1.7 ± 0.4	330 ± 100
	MeOH II	3.8 ± 0.8	59 ± 4	2.3 ± 0.8	500 ± 130

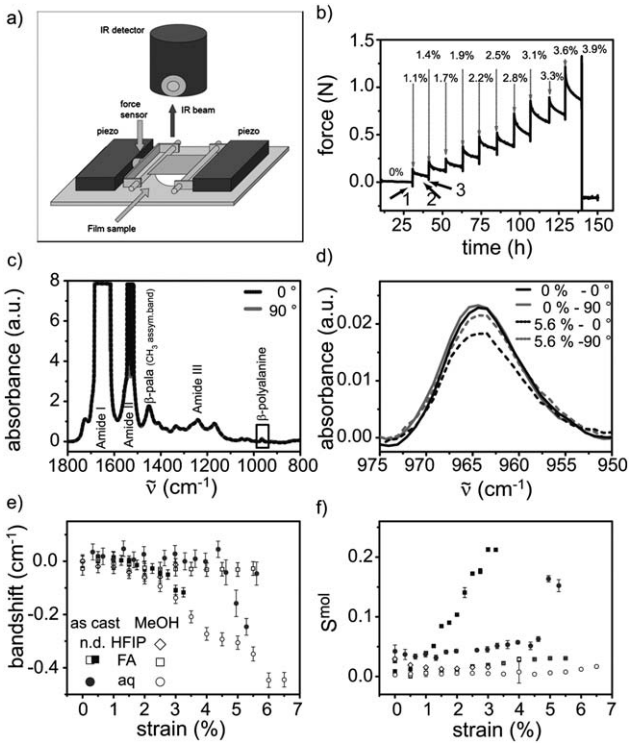

Fig. 6 Molecular orientation upon stretching. (a) Measurement setup for simultaneous mechanical and transmission mode IR measurements. The IR beam is focused on the film, and a sensor measures the applied force upon stretching the sample with micrometer screws.[30] Reproduced by permission of The Royal Society of Chemistry (RSC). (b) Example force curve obtained after stepwise strain increase (1). The sample was allowed to relax (2) (monitored by the force detector), followed by FTIR analysis (3). (c) IR absorption spectra of an eADF4(C16) film cast from FA measured before stretching with light polarized parallel (black dotted curve) and perpendicular (grey solid curve) with respect to the direction of applied stress. The results revealed no initial structural orientation in the film; (d) The spectral region between 975 and 945 cm^{-1} corresponds to polyalanines in β-sheet structures. As a representative example, this region is shown for aq films before (0%, solid line) and after 5.6% stretching (dotted line) with light polarized parallel (black) and perpendicular (grey) with respect to the direction of applied stress; (e) Response of the shift of the β-polyalanine absorption band at 964 cm^{-1} to external strain; (f) Molecular order parameter, S^{mol}, of β-polyalanine structures. Symbols as in (e).

940 and 975 cm^{-1} for notable reasons: (i) in contrast to the amide I region, where many components contribute, this peak can be assigned to amino acid specific bands; (ii) the amide I region showed (partially) high scattering in transmission mode (Fig. 6c); (iii) the polyalanine β-sheets have been reported to strictly contribute to the high stiffness of dragline silk, and thus they should reveal high dichroism/orientation of their vibration bond in response to mechanical stress. A quantum mechanical model has been previously employed to correlate stress with variation of the β-polyalanine vibration frequency, proving that the β-polyalanine main-chain vibration frequency varies linearly with stress and thus can be used as a force probe on the molecular level.[73] We analyzed the orientation, molecular order (S^{mol}), spectral position and the frequency width at half maximum (FWHM) of the β-polyalanine band during stretching. Negative bandshifts of the peak maxima were observed for films from buffered aqueous solution (*aq* films were measured in one piece, which did not allow differentiating between the two detected structural regions (types I and II)), as well as untreated FA films. In the case of the as cast FA and the methanol treated *aq* film, this bandshift occurred after a very low threshold of ~1% stretching. In the case of the as cast *aq* film, the threshold was 4.5%, indicating that the external stress is transduced to the monitored β-polyalanine structures, however, not immediately like in the case of dragline silk fibers,[27,73] but after a certain degree of stretching. In contrast, in methanol treated FA and HFIP films almost no bandshift was detected (Fig. 6e). The molecular order parameter S^{mol} increased from almost 0 (confirming the initial isotropic behavior of the film sample) to 0.18–0.22 in as cast films from aqueous solution and FA (Fig. 6f), indicating a partial orientation of the polyalanine β-sheet structures along the direction of stretching (a value of 1 would mean perfect alignment in this direction). S^{mol} increases with increasing strain after the identical (strain) threshold as detected in the bandshift, reflecting a direct relation of stretching and induced orientation of the monitored β-polyalanine absorption band. In contrast, no increase in S^{mol} was observed in all methanol treated films, which indicates that no reorientation of the β-polyalanines takes place. As no peak corresponding to β-polyalanines was detected in as cast HFIP films (Fig. 1b), changes in molecular orientation of polyalanine stretches in these films could not be analyzed.

Importantly, no induction of β-sheet structure was observed upon stretching in any of the films, as seen by the same overall absorbance at 964 cm^{-1} and at the amide I band (in the cases where scattering was not too high) throughout the whole experiment.

Impact of structural features on mechanical properties

The results presented above strongly indicate an influence of the used solvent on the mechanical properties of the films, not only in as cast films, but also after post-treatment with methanol. In the case of buffered aqueous solutions, inhomogeneity was detected in individual films concerning secondary structures and mechanical properties, most likely due to drying effects. In comparison to HFIP and FA, water is evaporating much slower, thereby presumably generating local differences in protein concentration which in turn influences intermolecular interaction. From general assembly studies of eADF4(C16) it is known that the kinetics of β-sheet formation is dependent on protein concentration and chain length.[83]

FTIR analysis suggests a direct correlation of mechanical behavior and protein secondary structure, with higher content of β-sheet leading to enhanced stiffness and strength. The interconnection of flexible chains and β-sheets has been described to determine the initial linear-elastic region of stress–strain curves.[69] A higher content in β-sheet structure results in stiffer materials, as it is intrinsically more rigid and also reduces the degree of freedom/mobility of the flexible parts by acting as physical crosslinks. This effect was observed upon treatment of all as cast silk films with methanol, which significantly increased the β-sheet content. In contrast, the films displaying the lowest β-sheet content (as cast HFIP and *aq* type I) revealed plastic behavior (Fig. 5), which can be assigned to deformation/disentangling of

chains after rupture of H-bonds in the flexible regions.[84,85] A tighter interconnection of the chains in all other films would prevent such deformation due to a higher amount of β-sheets by acting as rigid crosslinks.[51,85]

Interestingly, after methanol treatment, HFIP and *aq* type I films are the weakest and most brittle, which cannot be explained by the amount of β-sheets, but rather by a different arrangement of the β-strands and by a lower amount of interstitial solvent (water) molecules. From detailed molecular dynamic simulations, Buehler and co-workers concluded that there is a critical size and geometry of β-sheets beyond which stability decreases significantly.[86–88] Taking into account that the protein structure is initially largely determined by the solvent (HFIP has been described to stabilize α-helices[71,72]), it seems reasonable that methanol treatment/removal of HFIP induces quite abrupt and massive structural changes, which could lead to the formation of unfavorable structures (in terms of mechanical stability). In contrast, in films cast from other solvents the proteins can undergo a more "balanced" structural transition (Table 1). For example, the formation of long-range order crystallites upon methanol immersion has been shown to be restricted in FA films of regenerated *B. mori* SF.[46] Comparison of the glass transition in methanol treated HFIP films and methanol treated films out of the other solvents indicates a higher energy needed for gain in chain mobility in treated HFIP films. The strong influence of HFIP on the proteins' structure was also kept during stretching the as cast films, which did not result in induction of (polyalanine-) β-sheet structures. Molecular orientation/re-arrangement is most probably a complex process involving many interactions. Here, we focused on the β-polyalanine vibration band since it can be analyzed unambiguously without being affected by overlapping other signals.[30,73] Analysis of unstretched films cast from either solvent revealed random orientation (with a molecular order parameter S^{mol} close to 0). Indeed, no molecular orientation was expected, as during film casting no (external) trigger for anisotropy (like shear forces or an electrical field) was employed. Accordingly, no orientation is observed in untreated films from regenerated *B. mori* SF.[48,54] Once stress was applied, partial orientation of the polyalanine β-sheets along the direction of applied stress was observed in as cast films (FA and *aq*), with the molecular order parameter S^{mol} increasing with increasing strain. As such structure is absent, no further information could be obtained for as cast HFIP films. The detected alignment might be similar to the alignment and orientation of spider silk molecules during the spinning process, where shear forces and elongational flow constitute the trigger.[10] However, in contrast to a dragline silk fiber, where β-polyalanine crystals are almost perfectly aligned along the fiber axis (with a S^{mol} of 0.92[30]), S^{mol} reaches only a value of 0.2 in the films. Here, re-orientation is most likely limited by the molecular freedom within a complex and highly interconnected molecular network. Accordingly, none of the methanol treated films, which display elevated β-sheet contents compared to as cast films, revealed any gain in orientation, indicating that the β-sheets are too tightly connected or cross-linked.

The increase in S^{mol} was observed after a certain threshold of stretching, which coincided with a threshold in the shift in the peak maximum. Compared to a thresholdless transition of external stress to β-polyalanine crystals in dragline fibers,[27,30] this suggests a different molecular arrangement in the films, with the external stress leading to an initial extension of amorphous chains before the monitored β-polyalanine structures are affected. Then, the external stress is transduced to the polyalanine β-sheets, resulting in their partial orientation and altered vibrations. The later onset of threshold in the *aq* films reflects a higher amount of extendable structural elements. The observed re-arrangement might be similar to observations in sericin films, where it has been suggested that stretching stress propagates through H-bonds leading to an orientation of aggregated strands.[89] Orientation of crystalline β-sheets upon stretching has also been reported for silk SF films, however, there the drawing was done at elevated temperatures and involved also induction of new β-sheets.[54]

After methanol treatment, a significant shift in the peak maximum of β-polyalanines was only observed for *aq* films. The absence of a band-shift in methanol treated HFIP and FA films might reflect either the presence of chains bypassing polyalanine β-sheets[30] or the appearance of local H-bond ruptures (within β-sheets or at the interface between stiff/flexible regions).[85] Indeed, the abrupt relaxation seen in the force curves of methanol treated films (Fig. S2†) indicates a rapid dissipation of energy.

Importantly, the observed differences in molecular mobility (orientation of polyalanine β-sheets) cannot be solely explained by different water content in the films. Interstitial water is known to act as plasticizer,[55,90] and determination of the water content in our films revealed slightly decreased values (1–3%) in as cast films from HFIP and FA, while all other films showed similar water content (as determined from TGA and Karl–Fischer titrations, data not shown). Therefore, interstitial solvent molecules together with the β-sheet amount and arrangement are important for the film's properties.

Experimental

Film preparation

The recombinant spider silk protein eADF4(C16) consists of 16 repeats of a module (sequence: GSSAAAAAAAASGPGGYGP ENQGPSGPGGYGPGGP) mimicking the monomeric unit which is repeated several times in the dragline protein ADF4.[34] Production in *E. coli* and purification were performed as described previously.[34] For film preparation, lyophilized protein was either directly dissolved in 1,1,1,3,3,3-hexafluoro-2-propanol (HFIP) or formic acid, or dissolved in guanidinium thiocyanate (6 M) followed by dialysis against aqueous buffer (5 mM NH_4HCO_3, pH 8). After dialysis, the solution was centrifuged (55.000 rpm, 60 min), and the protein concentration was adjusted to 2.5–3 mg ml^{-1}. If not stated otherwise, the solution was cast onto polystyrene Petri dishes and left to evaporate in a chamber with controlled relative humidity of 30%. After complete drying, films were either analyzed directly (as cast) or post-treated with methanol overnight and analyzed after complete evaporation of methanol.

Fourier transform infrared (FTIR) spectroscopy

FTIR spectra of films were recorded by attenuated total reflection (ATR) with a Bruker Tensor 27 spectrometer (Bruker, Germany) equipped with a *Ge* crystal. To eliminate spectral

contributions due to atmospheric water vapour, the instrument was purged with dry air and atmospheric compensation was performed. For each measurement, 100 scans with a resolution of 2 cm^{-1} were averaged. To determine individual secondary structure components, the amide I band was analyzed by Fourier self deconvolution (FSD) as described in ref. 51 using the Opus 6.5 software from Bruker Optics Corp. (Billerica, MA, USA). After narrowing the band synthetically using a high pass filter, the resulting deconvoluted spectra were curve-fitted by subsequent Gaussian peaks. The fraction of individual secondary structure elements was calculated from the relative peak areas. Individual bands were assigned to the different secondary structure elements according to ref. 51. Spectra from at least three independent samples were averaged.

In order to study the changes of the molecular structure upon external strain, mechanical and time resolved polarized FTIR spectroscopy were combined. For these FTIR measurements the setup was used as shown in Fig. 6a. A Varian FTIR spectrometer was used with a photovoltaic MCT detector (KMPV50, Kolmar Technologies) working in the range from 750 to 5000 cm^{-1} at a nominal resolution of 4 cm^{-1}, with 1024 scans being averaged. A KRS-5 IR polarizer was inserted in the IR beam to study the dichroism. The spectrometer was coupled with a microscope working in transmission mode. The samples were glued to the apparatus using a two component epoxy adhesive and stretched stepwise (Fig. 6a). After relaxation of the sample (as seen by the force signal), rapid-scan measurements were carried out under equilibrium (Fig. 6b). The force applied to the sample during IR measurements was measured using a sensor (Buster GmbH) capable of measuring up to 10 N.

FTIR data analysis

FTIR bands were fitted with a sum of Gaussian profiles. A simple straight baseline was subtracted. Simultaneous fits were made for all polarization directions at a given strain value.

Transmittance varies sinusoidally with polarization; therefore, the absorbance was fitted with the following equation:

$$A(\theta) = -\log_{10}\left(10^{-A_x}\cos^2\theta + 10^{-A_y}\sin^2\theta\right) \quad (1)$$

where A_x and A_y are the absorbance values with light polarized parallel to the x (along the direction of applied force) and y (perpendicular to direction of applied force) axes, respectively, and θ is the polarization angle measured from the x-direction (film axis).

The molecular order parameter can be calculated as:

$$S^{mol} = (A_x - A_y)/(A_x + 2A_y) \quad (2)$$

Perfectly aligned transition dipole moments along the x-directions give a value of 1, whereas the molecular order parameter for isotropic samples is equal to zero.

Solid state NMR

Solid state ^{13}C cross-polarization magic angle spinning (CP/MAS) NMR spectra were obtained with a commercial Avance II 300 Bruker spectrometer equipped with a standard triple resonance MAS probe. Silk protein films were pulverized and packed into 4 mm cubic zirconium rotors and spun at 5 kHz rotation frequency. All spectra were acquired at room temperature and referenced to TMS using the external standard Adamantine. Simultaneous ^{1}H and ^{19}F broadband decoupling employed a SPINAL-64[66] and XiX[67] sequence, respectively, with an approximate nutation frequency of 50 kHz and 70 kHz. In order to allow a more complete assignment of the ^{13}C MAS spectra, a series of cross-polarization polarization inversion (CPPI) spectra[68] were additionally recorded with the purpose of distinguishing between overlapping spectra and differentiating between C, –CH, CH_2, and $–CH_3$ units.

Thermogravimetric analysis (TGA)

Changes in mass upon heating were assessed by TGA using a SDTA 851e Thermo-gravimetric Analyzer (Mettler Toledo, Germany) with a microbalance resolution of 1 μg. Measurements were done in aluminium oxide pans under nitrogen atmosphere (50 ml min^{-1}) at a heating rate of 10 °C min^{-1} (from RT to 800 °C). The shown graphs are representative of three individual measurements.

Differential scanning calorimetry (DSC)

DSC scans were obtained using a SDTA 821e differential scanning calorimeter (Mettler Toledo, Germany) with a ceramic sensor with 56-fold Au–AuPd thermocouple pile. Samples (3–4 mg) were sealed hermetically in aluminium pans and heated under purged dry nitrogen gas flow (20 ml min^{-1}) at 5 °C min^{-1}. In order to evaporate residual solvent, samples were first heated up to 110 °C. After 10 min of equilibration they were cooled to −40 °C, and, finally, the analysis was started by heating up to 400 °C. The shown graphs are representative of two or three individual measurements.

Tensile testing

Tensile testing was performed using an Instron universal tester 5565 (Instron, Norwood, MA, USA) equipped with a 10 N capacity load cell, which worked with a deviation ≤0.2% in the relevant load regime. A crosshead speed of 0.2 mm min^{-1} was applied, and gauge length was set to 10 mm. All films were tested in dry state at a relative humidity between 41 ± 1% at 20 ± 1 °C. Films were cut into strips of 1.5–2 mm × 20 mm. The thickness was individually determined for each sample and ranged from 10 to 12 μm (apart from film edges). Stress was calculated as force per cross-sectional area. Young's modulus (E-modulus) was measured from the initial slopes in the elastic region; tensile strength refers to the average of ultimate (engineered) stress at failure. Toughness was calculated as the integral below the respective stress–strain curve. The given values in Table 4 are averaged from 8 to 14 individual samples each (untreated films) and of 5 individual samples each (methanol treated films).

Conclusions

A systematic analysis of eADF4(C16) films was performed in order to assess the influence of different solvents on film properties. The used solvents (HFIP, FA and aqueous solution) had no remarkable effect on the films' thermal stability. Thermal

decomposition started around 270 °C with a maximum at 320 °C. In contrast, secondary structure content and mechanical characteristics revealed a clear dependence on the initial solvent used, with the effect on mechanics being sustained even after methanol treatment. Importantly, in the case of *aq* films local structural inhomogeneity appeared. Tensile testing as well as combined mechanical/structural analysis indicated differences not only due to post-treatment with methanol, but also due to the initial solvent. Taken together, the presented data give insights into the structure–function relationship of eADF4(C16) in films, which is an important basis for potential future applications. Furthermore, they broaden the understanding of the correlation of mechanical behavior and underlying molecular arrangement. The results clearly demonstrate that not only the amount of β-sheet structures has to be considered but also their arrangement (size/geometry and interconnection) in combination with interstitial solvent molecules. All factors are influenced by the chosen starting solvent, which thereby provides an additional parameter of controlling and fine-tuning the properties of silk materials.

Acknowledgements

This work was financially supported by SFB840 TPA8. The authors thank Dr Reiner Giesa (University of Bayreuth) for support on tensile testing and Ute Kuhn (University of Bayreuth) for DSC and TGA measurements.

Notes and references

1 K. Spiess, A. Lammel and T. Scheibel, *Macromol. Biosci.*, 2010, **10**, 998–1007.
2 A. R. Murphy and D. L. Kaplan, *J. Mater. Chem.*, 2009, **19**, 6443–6450.
3 J. A. Kluge, O. Rabotyagova, G. Leisk and D. L. Kaplan, *Trends Biotechnol.*, 2008, **26**, 244–251.
4 C. Vepari and D. L. Kaplan, *Prog. Polym. Sci.*, 2007, **32**, 991–1007.
5 D. H. Kim, J. Viventi, J. J. Amsden, J. Xiao, L. Vigeland, Y. S. Kim, J. A. Blanco, B. Panilaitis, E. S. Frechette, D. Contreras, D. L. Kaplan, F. G. Omenetto, Y. Huang, K. C. Hwang, M. R. Zakin, B. Litt and J. A. Rogers, *Nat. Mater.*, 2010, **9**, 511–517.
6 C. L. Craig, *Annu. Rev. Entomol.*, 1997, **42**, 231–267.
7 F. Vollrath and D. Porter, *Soft Matter*, 2006, **2**, 377–385.
8 Y. Z. Wang, H. J. Kim, G. Vunjak-Novakovic and D. L. Kaplan, *Biomaterials*, 2006, **27**, 6064–6082.
9 J. G. Hardy, L. M. Romer and T. R. Scheibel, *Polymer*, 2008, **49**, 4309–4327.
10 M. Heim, D. Keerl and T. Scheibel, *Angew. Chem., Int. Ed.*, 2009, **48**, 3584–3596.
11 J. M. Gosline, P. A. Guerette, C. S. Ortlepp and K. N. Savage, *J. Exp. Biol.*, 1999, **202**, 3295–3303.
12 F. Vollrath and D. P. Knight, *Nature*, 2001, **410**, 541–548.
13 C. Riekel and F. Vollrath, *Int. J. Biol. Macromol.*, 2001, **29**, 203–210.
14 A. D. Parkhe, S. K. Seeley, K. Gardner, L. Thompson and R. V. Lewis, *J. Mol. Recognit.*, 1997, **10**, 1–6.
15 A. Glisovic, T. Vehoff, R. J. Davies and T. Salditt, *Macromolecules*, 2008, **41**, 390–398.
16 J. D. van Beek, S. Hess, F. Vollrath and B. H. Meier, *Proc. Natl. Acad. Sci. U. S. A.*, 2002, **99**, 10266–10271.
17 A. H. Simmons, C. A. Michal and L. W. Jelinski, *Science*, 1996, **271**, 84–87.
18 T. Lefevre, M. E. Rousseau and M. Pezolet, *Biophys. J.*, 2007, **92**, 2885–2895.
19 J. Sirichaisit, V. L. Brookes, R. J. Young and F. Vollrath, *Biomacromolecules*, 2003, **4**, 387–394.
20 F. Vollrath and D. P. Knight, *Int. J. Biol. Macromol.*, 1999, **24**, 243–249.
21 M. Xu and R. V. Lewis, *Proc. Natl. Acad. Sci. U. S. A.*, 1990, **87**, 7120–7124.
22 C. Y. Hayashi, N. H. Shipley and R. V. Lewis, *Int. J. Biol. Macromol.*, 1999, **24**, 271–275.
23 E. Bini, D. P. Knight and D. L. Kaplan, *J. Mol. Biol.*, 2004, **335**, 27–40.
24 M. Heim, L. Romer and T. Scheibel, *Chem. Soc. Rev.*, 2010, **39**, 156–164.
25 D. T. Grubb and G. Ji, *Int. J. Biol. Macromol.*, 1999, **24**, 203–210.
26 G. P. Holland, M. S. Creager, J. E. Jenkins, R. V. Lewis and J. L. Yarger, *J. Am. Chem. Soc.*, 2008, **130**, 9871–9877.
27 P. Papadopoulos, R. Ene, I. Weidner and F. Kremer, *Macromol. Rapid Commun.*, 2009, **30**, 851–857.
28 P. Papadopoulos, J. Solter and F. Kremer, *Colloid Polym. Sci.*, 2009, **287**, 231–236.
29 B. L. Thiel, K. B. Guess and C. Viney, *Biopolymers*, 1997, **41**, 703–719.
30 R. Ene, P. Papadopoulos and F. Kremer, *Soft Matter*, 2009, **5**, 4568–4574.
31 C. Vendrely and T. Scheibel, *Macromol. Biosci.*, 2007, **7**, 401–409.
32 A. Rising, M. Widhe, J. Johansson and M. Hedhammar, *Cell. Mol. Life Sci.*, 2011, **68**, 169–184.
33 X. X. Xia, Z. G. Qian, C. S. Ki, Y. H. Park, D. L. Kaplan and S. Y. Lee, *Proc. Natl. Acad. Sci. U. S. A.*, 2010, **107**, 14059–14063.
34 D. Huemmerich, C. W. Helsen, S. Quedzuweit, J. Oschmann, R. Rudolph and T. Scheibel, *Biochemistry*, 2004, **43**, 13604–13612.
35 S. Rammensee, U. Slotta, T. Scheibel and A. R. Bausch, *Proc. Natl. Acad. Sci. U. S. A.*, 2008, **105**, 6590–6595.
36 F. Hagn, L. Eisoldt, J. G. Hardy, C. Vendrely, M. Coles, T. Scheibel and H. Kessler, *Nature*, 2010, **465**, 239–242.
37 G. Askarieh, M. Hedhammar, K. Nordling, A. Saenz, C. Casals, A. Rising, J. Johansson and S. D. Knight, *Nature*, 2010, **465**, 236–238.
38 X. Y. Wang, X. Hu, A. Daley, O. Rabotyagova, P. Cebe and D. L. Kaplan, *J. Controlled Release*, 2007, **121**, 190–199.
39 X. Wang, E. Wenk, X. Hu, G. R. Castro, L. Meinel, X. Wang, C. Li, H. Merkle and D. L. Kaplan, *Biomaterials*, 2007, **28**, 4161–4169.
40 E. Wenk, A. J. Meinel, S. Wildy, H. P. Merkle and L. Meinel, *Biomaterials*, 2009, **30**, 2571–2581.
41 J. J. Amsden, P. Domachuk, A. Gopinath, R. D. White, L. D. Negro, D. L. Kaplan and F. G. Omenetto, *Adv. Mater.*, 2010, **22**, 1746–1749.
42 B. D. Lawrence, M. Cronin-Golomb, I. Georgakoudi, D. L. Kaplan and F. G. Omenetto, *Biomacromolecules*, 2008, **9**, 1214–1220.
43 K. Spiess, S. Wohlrab and T. Scheibel, *Soft Matter*, 2010, **6**, 4168–4174.
44 C. Zhao, J. Yao, H. Masuda, R. Kishore and T. Asakura, *Biopolymers*, 2003, **69**, 253–259.
45 S. W. Ha, A. E. Tonelli and S. M. Hudson, *Biomacromolecules*, 2005, **6**, 1722–1731.
46 I. C. Um, H. Y. Kweon, K. G. Lee and Y. H. Park, *Int. J. Biol. Macromol.*, 2003, **33**, 203–213.
47 A. Vasconcelos, G. Freddi and A. Cavaco-Paulo, *Biomacromolecules*, 2008, **9**, 1299–1305.
48 H. J. Jin, J. Park, V. Karageorgiou, U. J. Kim, R. Valluzzi and D. L. Kaplan, *Adv. Funct. Mater.*, 2005, **15**, 1241–1247.
49 U. Slotta, M. Tammer, F. Kremer, P. Koelsch and T. Scheibel, *Supramol. Chem.*, 2006, **18**, 465–471.
50 M. Tsukada, Y. Gotoh, M. Nagura, N. Minoura, N. Kasai and G. Freddi, *J. Polym. Sci., Part B: Polym. Phys.*, 1994, **32**, 961–968.
51 X. Hu, D. Kaplan and P. Cebe, *Macromolecules*, 2006, **39**, 6161–6170.
52 O. N. Tretinnikov and Y. Tamada, *Langmuir*, 2001, **17**, 7406–7413.
53 J. Yin, E. Chen, D. Porter and Z. Shao, *Biomacromolecules*, 2010, **11**, 2890–2895.
54 T. Yucel, P. Cebe and D. L. Kaplan, *Adv. Funct. Mater.*, 2011, **21**, 779–785.
55 A. Motta, L. Fambri and C. Migliaresi, *Macromol. Chem. Phys.*, 2002, **203**, 1658–1665.
56 A. Lammel, X. Hu, S. H. Park, D. L. Kaplan and T. Scheibel, *Biomaterials*, 2010, **31**, 4583–4591.
57 A. Lammel, M. Schwab, M. Hofer, G. Winter and T. Scheibel, *Biomaterials*, 2011, **32**, 2233–2240.
58 D. Huemmerich, U. Slotta and T. Scheibel, *Appl. Phys. A: Mater. Sci. Process.*, 2006, **82**, 219–222.
59 E. Metwalli, U. Slotta, C. Darko, S. V. Roth, T. Scheibel and C. M. Papadakis, *Appl. Phys. A: Mater. Sci. Process.*, 2007, **89**, 655–661.
60 F. Junghans, M. Morawietz, U. Conrad, T. Scheibel, A. Heilmann and U. Spohn, *Appl. Phys. A: Mater. Sci. Process.*, 2006, **82**, 253–260.

61 J. S. Stephens, S. R. Fahnestock, R. S. Farmer, K. L. Kiick, D. B. Chase and J. F. Rabolt, *Biomacromolecules*, 2005, **6**, 1405–1413.
62 E. Bini, C. W. P. Foo, J. Huang, V. Karageorgiou, B. Kitchel and D. L. Kaplan, *Biomacromolecules*, 2006, **7**, 3139–3145.
63 M. Widhe, H. Bysell, S. Nystedt, I. Schenning, M. Malmsten, J. Johansson, A. Rising and M. Hedhammar, *Biomaterials*, 2010, **31**, 9575–9585.
64 A. W. Morgan, K. E. Roskov, S. Lin-Gibson, D. L. Kaplan, M. L. Becker and C. G. Simon, *Biomaterials*, 2008, **29**, 2556–2563.
65 C. W. P. Foo, S. V. Patwardhan, D. J. Belton, B. Kitchel, D. Anastasiades, J. Huang, R. R. Naik, C. C. Perry and D. L. Kaplan, *Proc. Natl. Acad. Sci. U. S. A.*, 2006, **103**, 9428–9433.
66 B. M. Fung, A. K. Khitrin and K. Ermolaev, *J. Magn. Reson.*, 2000, **142**, 97–101.
67 M. Ernst, A. Samoson and B. H. Meier, *J. Magn. Reson.*, 2003, **163**, 332–339.
68 B. Jurgens, E. Irran, J. Senker, P. Kroll, H. Muller and W. Schnick, *J. Am. Chem. Soc.*, 2003, **125**, 10288–10300.
69 O. S. Rabotyagova, P. Cebe and D. L. Kaplan, *Macromol. Biosci.*, 2010, **10**, 49–59.
70 A. Barth, *Biochim. Biophys. Acta*, 2007, **1767**, 1073–1101.
71 K. Gast, A. Siemer, D. Zirwer and G. Damaschun, *Eur. Biophys. J.*, 2001, **30**, 273–283.
72 F. D. Sonnichsen, J. E. Van Eyk, R. S. Hodges and B. D. Sykes, *Biochemistry*, 1992, **31**, 8790–8798.
73 P. Papadopoulos, J. Solter and F. Kremer, *Eur. Phys. J. E: Soft Matter Biol. Phys.*, 2007, **24**, 193–199.
74 J. Ashida, K. Ohgo and T. Asakura, *J. Phys. Chem. B*, 2002, **106**, 9434–9439.
75 H. Saito, R. Tabeta, A. Shoji, T. Ozaki, I. Ando and T. Miyata, *Biopolymers*, 1984, **23**, 2279–2297.
76 Y. Gotoh, M. Tsukada, T. Baba and N. Minoura, *Polymer*, 1997, **38**, 487–490.
77 N. Agarwal, D. A. Hoagland and R. J. Farris, *J. Appl. Polym. Sci.*, 1997, **63**, 401–410.
78 X. Hu, D. Kaplan and P. Cebe, *Macromolecules*, 2008, **41**, 3939–3948.
79 C. Y. Jiang, X. Y. Wang, R. Gunawidjaja, Y. H. Lin, M. K. Gupta, D. L. Kaplan, R. R. Naik and V. V. Tsukruk, *Adv. Funct. Mater.*, 2007, **17**, 2229–2237.
80 X. Chen, Z. Z. Shao and F. Vollrath, *Soft Matter*, 2006, **2**, 448–451.
81 C. Riekel, B. Madsen, D. Knight and F. Vollrath, *Biomacromolecules*, 2000, **1**, 622–626.
82 J. Perez-Rigueiro, M. Elices, G. Plaza, J. I. Real and G. V. Guinea, *J. Exp. Biol.*, 2005, **208**, 2633–2639.
83 U. K. Slotta, S. Rammensee, S. Gorb and T. Scheibel, *Angew. Chem., Int. Ed.*, 2008, **47**, 4592–4594.
84 Y. Termonia, *Macromolecules*, 1994, **27**, 7378–7381.
85 S. Keten and M. J. Buehler, *J. R. Soc., Interface*, 2010, **7**, 1709–1721.
86 S. Keten and M. J. Buehler, *Nano Lett.*, 2008, **8**, 743–748.
87 S. Keten, Z. Xu, B. Ihle and M. J. Buehler, *Nat. Mater.*, 2010, **9**, 359–367.
88 N. Du, Z. Yang, X. Yang Liu, Y. Li and H. Yao Xu, *Adv. Funct. Mater.*, 2011, **21**, 772–778.
89 H. Teramoto and M. Miyazawa, *Biomacromolecules*, 2005, **6**, 2049–2057.
90 N. Minoura, M. Tsukada and M. Nagura, *Biomaterials*, 1990, **11**, 430–434.

